Dynamic simulations of many-body electrostatic self-assembly

Eric B. Lindgren[1], Benjamin Stamm[2], Yvon Maday[3,4,5,6], Elena Besley[1] and A. J. Stace[1]

[1]Department of Physical and Theoretical Chemistry, School of Chemistry, University of Nottingham, University Park, Nottingham NG7 2RD, United Kingdom.
[2]Centre for Computational Engineering, Mathematics Department, RWTH Aachen University, Schinkelstr. 2, 52062 Aachen, Germany.
[3]Sorbonne Universités, UPMC Univ Paris 06, UMR 7598, Laboratoire Jacques-Louis Lions, F-75005, Paris, France.
[4]CNRS, UMR 7598, Laboratoire Jacques-Louis Lions, F-75005, Paris, France.
[5]Institut Universitaire de France.
[6]Brown University, Division of Applied Mathematics, Providence, RI, USA.

Abstract

Two experimental studies relating to electrostatic self-assembly have been the subject of dynamic computer simulations, where the consequences of changing the charge and the dielectric constant of the materials concerned have been explored. One series of calculations relates to experiments on the assembly of polymer particles that have been subjected to tribocharging and the simulations successfully reproduce many of the observed patterns of behaviour. A second study explores events observed following collisions between single particles and small clusters composed of charged particles derived from a metal oxide composite. As before, observations recorded during the course of the experiments are reproduced by the calculations. One study in particular reveals how particle polarisability can influence the assembly process.

Keywords: many-body, electrostatic, self-assembly, simulations, particles.

1. Introduction

The electrostatic self-assembly of particles has become an important and effective route to the synthesis of structured materials, many with unique optical, magnetic or mechanical properties [1-5]. By utilizing particulate components carrying charges of opposite sign, it has become possible to assemble two- and three-dimensional structures from a wide range of dielectric and conducting particles [6-9]. A cursory search of the literature reveals a steady year-on-year increase in the number of experimental papers devoted to this topic, with almost 8,000 publications in the past ten years. In many respects, theory has failed to keep pace with the numerous and innovative developments in experimentation. The very close proximity of large numbers of assembled charged particles requires a knowledge of electrostatic interactions beyond the two-body problem, with the non-additivity of forces involving polarisable dielectric and/or conducting particles necessitating the application of a many-body theory [10-17]. However, using the many-body approach just to predict minimum energy structures does not necessarily mimic the assembly process, where particles are free to explore numerous confirmations and metastable geometries, each possibly having their own set of interesting properties. The alternative approach, whereby the dynamics of electrostatic self-assembly process is modelled introduces one over-riding problem, namely, computational complexity. The long-range nature of the Coulomb interaction requires that forces be evaluated well beyond the immediate vicinity of any particular charged particle. In addition, a proper account of polarisation effects is needed since the induction of bound charge on one particle is coupled to the same process on all others. Hence, summations need to be taken over the manifold of terms in, for example, a multipole description of the electrostatic interactions present in any collection of polarisable neutral and charged particles. Coupled with this is the added requirement that any dynamical study of M particles requires the simultaneous solving of 6 M equations of

motion at each time step in a simulation. To date, there have been a number of "coarse grain" studies where the Dissipative Particle Dynamics (DPD) technique has been used to simulate a range of electrostatic assembly processes [18-24]. For the most part these studies have used pair potentials; however, in a related study, Dahirel *et al*. [25,26] have used an interaction potential that included three-body terms to study the dynamical behaviour of charged particles in aqueous solutions of electrolytes. The introduction of electrostatic forces into DPD derives from the work of Groot [27] and more recently, Gavrilov *et al.* have extended these ideas to particulate systems with high charge densities [28].

Presented here are initial results from a series of calculations where an integral equation approach has been used to calculate many-body electrostatic interactions between charged particles, and for large numbers of particles a linear scaling has been achieved through the use of a fast multipole method. This approach has been combined with a method for solving the classical equations of motion to give time-dependent images of charged particle assembly processes. To link the simulations to experimental data, two separate series of quite different experiments have been identified where electrostatic assembly has been promoted in the absence of additional constraints, such as the presence of a solvent or ionic medium. Whitesides and co-workers have made extensive use of contact electrification to create two-dimensional models of electrostatic self-assembly [29-33]. Collections of millimetre-sized polymer spheres of varying size and composition, i.e. Nylon, Teflon etc. have been subjected to tribocharging, whereby they acquired either a positive or negative charge of the order of a few hundred pico-Coulombs (pC). As a consequence of the resultant electrostatic interactions, the spheres self-organised into a range of lattice structures [29-33]. In a second series of experiments, Lee *et al*. [34] succeeded in capturing images of submillimetre-sized particles clustering in charged granular streams. Time sequences of particle motion in a vacuum and under gravitational force showed examples of orbiting binary collisions and clustering events

where one charged particle collides with and can eventually attach itself to a pre-existing stable collection of particles. These experiments differ from those of Whitesides and co-workers in several ways: first, the particles were smaller (~ 300 μm) and carried less charge (~ 0.1pC), but more significantly, the material used, a composite of zirconium dioxide and silicate, has a much higher dielectric constant than any of the polymer spheres used by Whitesides and co-workers [29-33]. From the composition of the ZrO_2/SiO_2 particles, Lee *et al*. [34] estimated the dielectric constant to be approximately 15, which is to be compared with values of between 2 and 4 for the polymer particles. Both these studies have been the subject of a series of computer simulations where attempts have been made to reproduce the collision dynamics that ultimate leads to the experimental observation of assembled structures [29-34]. Although the fabrication of many devices [1-9] can involve (nano) particles that are much smaller than those studied here, it can be shown through scaling relationships [35], that as a function of their charge to size ratio, there is a direct correspondence between forces predicted for any given collection of charged spheres, and those that will be present in either a larger or smaller system.

2. Theory

A three-dimensional geometric representation of the system to be simulated is illustrated in figure 1, which shows a collection of M non-over lapping charged dielectric spheres, Ω_1 - Ω_M. Each particle is centred at a position given by $x_i \in \mathbb{R}^3$, has a radius r_i and a dielectric constant k_i. All particles are suspended in a homogeneous medium of dielectric constant k_0, which defines a boundary interface, $\Gamma_i = \partial\Omega_i$ between each Ω_i (i=1,…,M) and the medium Ω_0 (air or vacuum in the present case), and where $\Gamma_0 = \Gamma_1 \cup ... \cup \Gamma_M$.

Each particle carries a free charge q_i, uniformly distributed over its surface and represented by a surface charge density $\sigma_{f,i} = q_i/(4\pi r_i^2) \in \mathbb{R}$. Let σ_f denote a global function, such that:

$$\sigma_f(x) = \begin{cases} \sigma_{f,i} & \text{if } x \in \Gamma_i \\ 0 & \text{otherwise} \end{cases}$$

The electrostatic potential Φ created by the density of free charge σ_f residing on the particles satisfies standard boundary conditions in electrostatics:

$$\begin{aligned} \Delta\Phi &= 0 && \text{in each } \Omega_i, i = 0, 1, \dots, M, \\ [\![\Phi]\!] &= 0 && \text{on } \Gamma_0, \\ [\![k\nabla\Phi]\!] &= 4\pi K\sigma_f && \text{on } \Gamma_0, \end{aligned}$$

where *K* is Coulomb's constant and $[\![\Phi]\!]$ and $[\![k\nabla\Phi]\!]$ are discontinuities across each interface. If Φ can be determined, then the electrostatic energy *U* follows directly from [36,37]

$$U(\Phi, \sigma_f) = \frac{1}{2}\int_{\Gamma_0} \sigma_f(s)\Phi(s)ds \qquad (1)$$

where $s \in \Gamma_0$. As presented elsewhere [17], an integral equation that uniquely represents Φ for a global charge density σ_f can be derived and a solution obtained through a discretisation based on numerical integration in the space of truncated spherical harmonics. The resultant set of linear equations can be solved iteratively. The total electrostatic energy of the system can be obtained from Eq. 1 and the net electrostatic force on each particle, Ω_i, comes as the gradient of the energy with respect to changes in x_i (i=0,1,….M). For examples that involve large numbers of particles, resolution of the linear system benefits from the implementation of a fast multipole method (FMM), which provides an effective linear scaling of computational time with respect to the number of particles [17].

In this paper a comparatively simple (first-order) dynamic model has been adopted for the purposes of identifying gross features that might contribute to a better qualitative understanding of events leading up to the self-assembly of charged particles. Simulations consisted of fixed numbers of non-overlapping particles, each with an assigned dielectric constant, charge, radius, and mass. At the start of simulations which explored the experiments by Whitesides and co-workers [29-33], the particles were allocated a position and a velocity in a simulated box with rigid walls. The initial placement of particles within the box was the same in each simulation and was been chosen to avoid any bias in the outcome towards a particular final geometry. For simulations of the experiments by Lee *et al.*[34], single and collections of particles were suspended in isolation under a gravitational force.

The total electromagnetic force between any pair of interacting charged particles can be obtained from [38]:

$$\mathbf{F}_{12} = K\frac{q_1 q_2}{h^2}\left[\hat{\mathbf{h}} + \frac{\mathbf{v}_2\times(\mathbf{v}_1\times\hat{\mathbf{h}}}{c^2}\right] \qquad (2)$$

where $\mathbf{v}_i$ is the velocity of particle i and c is the speed of light. Since the velocities of the particles in these simulations were very much lower than c, the second term in the brackets is very small and so can be neglected. Therefore, all interactions are accurately represented just from a consideration of electric components to the electromagnetic force. The set of first-order differential equations representing the classical equations of motion have been solved using the Euler method [39], where the computational routine included a collision handler to ensure that particles did not overlap.

To facilitate assembly, a frictional component or coefficient of restitution (CR) has been incorporated into the equations of motion, in such a way that linear momentum is conserved, but some fraction of the kinetic energy is dissipated at each collision:

$$\mathrm{CR} = \frac{\text{relative speed after a collision}}{\text{relative speed before a collision}}$$

Values assigned to CR have been taken from experimental measurements [34,40], some of which were the subject of these simulations [34]. Although the particle trajectories were dissipative, for a number of reasons the computations described here differ significantly from the electrostatic DPD studies discussed in the Introduction [18-28] and from DPD studies in general [41,42]. First, the number of particles involved in each simulation was sufficiently small that no attempt was made to consider the system as constituting a canonical (*NVT*) ensemble through the assignment of a temperature. Therefore, the pair-wise CR or frictional force was not balanced by any random temperature-dependent force acting as a heat source or sink [42]. This omission was helped by the fact that in all close encounters between charged particles $U >> k_B T$, where k_B is the Boltzmann constant and T is a temperature. In addition, both experiments were undertaken in the presence of an external force, which was either mechanical [29-33] or gravitational [34]. Furthermore, a many-body electrostatic theory has been used to describe charged particle – neutral particle and charged particle – charged particle interactions, whereas DPD studies have used pair potentials within a "smeared charge" formalism to avoid problems with point charges [20,23,24,27,28]. Finally, the experiments being reproduced have been undertaken in either vacuum or air, hence there was no electrolyte present, and therefore, no charge screening.

3. Results and discussion

The calculations began by exploring how the collision dynamics might be influenced by the two key parameters, namely dielectric constant and CR. Two particles with nominal radii $r_1 = r_2 = 1$, nominal charges $q_1 = 1$ and $q_2 = 0$, and nominal masses $m_1 = m_2 = 1$ were assigned the

starting coordinates $(x_{1,x},x_{1,y},x_{1,z})$ = (0,0,0) and $(x_{2,x},x_{2,y},x_{2,z})$ = (3,0,0) and the trajectories allowed to evolve from rest. Apart from when k_i = 1, these starting conditions ensured the particles were always trapped within an attractive electrostatic potential.

Figure 2a illustrates the consequences a change in dielectric constant has on the particle-particle interaction energy as a function of time. At one extreme, k_i = 1 represents a hard sphere collision between a charged and a neutral non-polarizable particle for which there is no change in interaction energy during the course of a collision. At the other extreme, k_i = 80 leads to a strong, mutual polarization of bound charge on each of the particles [43], which in turn causes a rapid increase in magnitude of the interaction energy. Accompanying the latter is a noticeable increase in collision frequency, which is associated with the elastic encounters taking place at a comparatively high speed. To explore the impact of CR < 1, the trajectories shown in figure 2a were repeated with CR = 0.94 and the results presented in figure 2b. Changing the coefficient of restitution has two obvious consequences; first there is the expected decline in the interaction energy since each collision now dissipates some fraction of the collision energy and secondly, the collision frequency increases because the particles are no longer returning to their initial starting coordinates after each encounter. Both of these effects become more pronounced as the dielectric constant of the particles increases. Eventually, the two particles aggregate, but the timescale over which this happens is dependent on the dielectric constant, which in turn, could have additional for self-assembly processes.

(a) Simulation of experiments by Whitesides and co-workers

A generic experiment of the kind undertaken by Whitesides and co-workers consisted of a collection (~100-200) of polymer spheres with different compositions, for example poly(methy methacrylate (PMMA) and Teflon, being vigorously agitated in a square or circular dish to allow each type of sphere to acquire either a negative or positive charge through tribocharging

[29-33]; a process that appears to take approximately 100 s. As a consequence of their charge, the particles self-assembled into different two-dimensional lattice structures with geometries that could vary according to particle charge, size, and the fraction of each polymer type. The simulations began at the point where the particles were assumed to have acquired their maximum charge (as determined by experiments [29-33]) and then explored a limited range of the very extensive experimental parameter set (size, dish shape, dish composition, etc.) surveyed by Whitesides and co-workers [32]. In particular, the effects of varying the following physical parameters have been examined: particle charge, dielectric constant, and the ratio of the number of negatively and positively charged particles; in addition, the simulations made it possible to investigate changes in lattice geometry due to variations in the dielectric constant. Table 1 lists the physical characteristics assigned to each particle type, and specific variables, such as the sign and magnitude of the charge, are also identified in the text. In addition to the above, these many-body calculations have made it possible to investigate the influence the number of electrostatic multipole terms, N, has on the observed lattice structures.

Figure 3 shows the time evolution of a collection of equal numbers of PMMA spheres (yellow) and Teflon spheres (blue), with q=+0.31 nC on PMMA and q=-0.31 nC on Teflon, to give a system that is overall charge neutral. In this simulation N=4 and so the multipole interactions cover terms up to hexadecapole. As can be seen, after 2 s of simulation the system has assembled into a lattice structure that primarily consists of square arrangements of alternating PMMA and Teflon particles, which is similar to what is observed in an experiment where equal numbers of particles of the two polymer types each carry a charge of the same magnitude, but different sign [32]. The experiments also showed evidence of the enclosed gap seen in the simulation [32]. The differing colour shades within each sphere reflect subtle changes in the density of charge residing on the surface as a consequence of charge-induced polarisation. In the final image at 2 s it can be seen (green $\rightarrow$ yellow) that the more polarisable

PMMA particles exhibit an increase in charge density in the four regions where they are in closest contact with the Teflon particles. The Teflon particles, which are less polarisable, show a similar but weaker response. The numbers shown at the top of each frame correspond to the maximum values of the total surface charge density (nC mm^{-2}) at a particular time; at infinite separation, these numbers correspond to density of free charge. For the simulation shown in figure 3 the latter values for the total surface charge density are +0.01 nC mm^{-2} and -0.01 nC mm^{-2}. Since the free charge is fixed, any increase in charge density during the course of a simulation corresponds to a polarisation of bound charge, which in turn is reflected in the value of the dielectric constant. The largest fluctuations in charge density occur on the more polarisable PMMA particles. The final panel in figure 3 shows the changes that take place in the electrostatic interaction energy of the system (blue; in μJ) and the Root Mean Square (RMS) particle speed (red; in m s^{-1}) during the course of the simulation. The large drop in the electrostatic energy occurs because the system moves from an initial configuration that is very repulsive to one that is ultimately very attractive. The RMS speed starts from zero, rapidly increases because of particle – particle repulsion, but is then moderated by the coefficient of restitution and gradually drops towards zero as stable structures emerge.

Figure 4 describes the outcome of a simulation involving 36 PMMA and 12 Teflon particles, with the former carrying a charge of +0.31 nC and the latter -0.93 nC, which makes the simulation overall charge neutral. The equivalent surface charge densities are 0.01 nC mm^{-2} and -0.29 nC mm^{-2}, respectively at infinite separation. Experiments [29] showed that systems with this combination of characteristics resulted in the formation of a lattice that is predominantly hexagonal, but with the occasional pentagonal configuration. The same structures appear in the simulation after 2 s; but it is quite possible that the single pentagon is due to too few particles in the simulation rather than to deficiencies in the lattice dynamics. However, it is interesting to note that after 1.5 s of simulation, pentagonal configurations are

predominant, and that it is only after further relaxation that hexagonal geometries appear and begin to dominate. Compared with the previous example, the effect of increased free charge on the Teflon particles is to significantly enhance the magnitude of induced bound charge that appears of the surfaces of PMMA particles; however, through mutual polarisation, an equivalent charge density is induced on the Teflon particles [43,44]. Note the contrasting pattern of polarised charge density on the PMMA particles at the centre of the hexagonal lattice after 2 s, when compared with those in the square lattice seen in figure 4. If the simulation shown in figure 4 is repeated, but with k=1 (non-polarisable particles), then the average surface-to-surface separation between particles in the final lattice increases from 0.069 mm to 0.094 mm; however, these figures are of limited quantitative value as they will be very dependent on the numbers of each type of particle present.

From the last panel in figure 4 it can be seen that the final lattice energy is significantly lower than for the arrangement in figure 3, and although this is probably as a consequence of a much stronger, attractive Coulomb interaction, it is also evident from the final lattice geometry that there are a significant number of repulsive PMMA – PMMA interactions. However, even under circumstances where there is a strong repulsive Coulomb force between like-charged particles, any additional interactions arising from the polarisation of bound charge are always attractive and will serve to moderate repulsion [43,44]. Under favourable circumstance, such interactions can actually lead to like-charge attraction [45]. What most probably reflects an increase in particle – particle repulsion when compared with figure 3, is the RMS speed. In this case, the RMS drops rapidly, more so than in figure 3, but then as the PMMA particles begin to come into close proximity, mutual repulsion increases the electrostatic energy, and this is matched by a corresponding jump in the RMS speed. In fact the RMS reaches a value close to that seen at the very start of the previous simulation. In a final simulation of the Whitesides data [29-33], a system is examined that includes features taken from the two previous results.

Figure 5 shows the outcome of a simulation where there are 36 PMMA and 12 Teflon particles, with the former carrying a charge q=+0.31 nC, but the charge on the latter has been decreased to q=-0.31 nC. There are two consequences of this change; first, the final assembly seen after 2 s is, at best, very disordered with some evidence of transient trigonal and square arrangements where PMMA particles surround Teflon particles. It would appear that the charge on the Teflon particles is not sufficient to stabilise an extended lattice network of the type shown in figure 4. Secondly, positively charged particles (yellow) that are not part of a lattice are expelled to the boundaries of the container. Evidence for both these patterns of behaviour can be found in the experiments [32]. The inability of the system to stabilise can also be seen from a calculation of the electrostatic energy, which unlike the other two examples, remains positive throughout the simulation; however, it should be noted that an imbalance between the number of different particles means that the system has an overall positive charge. The final time snapshot corresponding to 2.0 s of simulation time, shows the presence of an alternating chain of PMMA and Teflon particles (top right in figure 5); a feature that has again been observed under certain experimental conditions [32], and can probably be attributed to attempts by the system to minimise particle-particle repulsion. When changes are made to the starting conditions of the system shown in figure 4, i.e. total number of particles and their initial positions, the simulations continue to reproduce the square coordination geometries seen after 2 s.

From this series of simulations, it would appear that configurations adopted by the charged particles are very sensitive to the relative numbers of negatively and positively charged particles and to the charge allocated to each particle. These qualitative conclusions closely match observations made during the course of experiments on the equivalent polymer particles. Although it is clear from figure 3-5 that bound charge it being polarised, this effect appears to have minimal influence on the dynamics and final geometries, which is probably a consequence of the polymer particles having low polarisabilities (dielectric constants).

(b) Simulation of experiments by Lee *et al.*

In a series of experiments designed to breakdown the self-assembly process into a sequence of single collisions between grains or particles, Lee *et al*. [34] have captured high resolution images of the individual collision events that contribute to the fabrication of a dielectric material. Individual and collections of isolated particles were allowed to free-fall in a vacuum chamber where single collision events were recorded using a high-speed video camera. As before, the particles became tribocharged, but this time as a result of the many collisions they experienced both during preparation and their passage through a grain hopper that feeds the vacuum chamber. The types of events that were observed between pairs of colliding species (individual particles and collections of two or more particles) depended on a slightly different set of variables to those considered above for the polymer particles. In addition to there being like- and oppositely-charged particles, the outcome of a collision also depended on the impact parameter and the centre-of-mass collision energy [46]; however, events are still moderated by the coefficient of restitution. Lee *et al.* [34] succeeded in capturing images corresponding to three types of event: (i) capture – where the centre-of-mass collision energy is either below the binding energy for a small cluster of particles, or is effectively dissipated in a larger collection; (ii) escape – where an incoming particle bounces away from a stable cluster; (iii) fragmentation – mainly seen at high collision energies and leads to the breakup of a cluster. The simulation of a collision between just two particles followed a sequence of multiply close encounters very similar to those shown in figure 2b, and where the application of a CR, ultimately led to a stable dimer (a pattern of behaviour that is also very similar to that depicted in Ref. 34, figure 1d). Since the particles have a comparatively high dielectric constant (k=15), the polarisation of bound charge made an important contribution towards stabilising the dimer, which at the point

of closest contact in the simulation had a total electrostatic energy of -8.26 pJ, of which induced interactions contributed -2.28 pJ.

The results that follow report on an examination of the conditions necessary for a cluster of charged particles to collide with and capture a single particle. The first set of simulations comprised of a cubic cluster of 4 negatively ($-5.2.10^6$e) and 4 positively ($+5.2.10^6$ e) charged particles in collision with a neutral particle. The values chosen for the charge are representative of those measured by Lee *et al.* [34], and equate to surface charge densities at infinite separation of ± 18.4 e μm^2 (note the change in units in order to identify with the data as presented [34]). Figure 6a shows a trajectory where none of the particles are polarisable (k=1) and the relative velocity between the initial aggregate and the colliding particle is 0.04 ms^{-1}. A collision with the *neutral* particle disrupts the aggregate for a short period (~ 100 ms), but the initial configuration is restored by a combination of strong Coulomb forces between oppositely charged constituent particles and the application of CR. As might be expected for a neutral, non-polarisable particle, the colliding particle is not captured, but is scattered away. Confirming the non-polarisable nature of the particles, the surface charge densities remains fixed at ± 18.4 eμm^2 throughout the trajectory. The final panel shows the interaction energy of the system, where it can be seen that prior to the collision at ~150 ms (denoted by a yellow circle) the eight-particle unit settles to a stable cubic structure. Following the collision the total energy increases rapidly, but the cube is slowly restored through the application of CR. In contrast, figure 6b shows the same trajectory, but this time with all particles assigned a value of k=15 and N=4. The maximum surface charge density on the cube is double that attributed to the free charge and as the trajectory evolves this increases to a factor of three. As a consequence of the enhanced polarizability, a collision with the neutral particle is far less disruptive and the particle is actually captured by the cluster. A quantitative summary of these events is given in

the final panel, where it can be seen that, prior to the collision, the energy of the initial cubic structure is significantly lower than that composed from non-polarisable particles.

Figure 7a shows a trajectory run with k=1 and where the relative velocity has been increased to 0.06 ms^{-1}. This time the collision has two consequences. First, it leads to a breakup of the cluster through the loss of a single particle, which the Coulomb forces are unable to prevent, and secondly, the remaining seven particles settle into a structure that appears to be a local energy minimum rather than the most stable unit. This pattern of behaviour is confirmed in the final panel where the interaction energy of the final structure is much higher than would be expected from a slightly reduced sum of pair potentials present in the starting geometry. Figure 7b shows the same trajectory, but with all the particles assigned a value of k=15. This time the colliding particle is scattered rather than captured by the cluster, and although the collision is very disruptive, the additional contributions from polarisation are effective in restoring the original composition, but not the starting structure of the eight-particle cluster. The final configuration formed at 800ms appears to occupy a local energy minimum with alternating positively and negatively charged spheres, with the less stable status being confirmed from a plot of the interaction energy. Figure 8a shows the outcome of a collision where the relative velocity has been increased to 0.08 ms^{-1} and this time the non-polarisable cluster experiences quite extensive disruption, with only pairs of oppositely-charged particles surviving. The same type of event with k=15 is shown in figure 8b, and although there is still extensive disruption, a core of the polarisable particles remains intact. Interestingly, the final structure formed after 400 ms has evolved into a chain which minimises repulsion by having alternate negatively and positively charged particles – an arrangement not unlike the chain configurations seen in figure 6 where the simulation also involved particles with charges of equal magnitude, but opposite sign. What is also interesting is that, of the final structures shown in figures 6-8, the chain structure shown in figure 8b is associated with a maximum in surface

charge density. However, the latter structure also displays a minimum number of contact points between oppositely charged particles, which means that bound charge is polarised in only one or two directions, rather than spread over 4, 5 or 6 contact points as seen in some of the more complex geometries present in figures 4 and 5.

Since it is very unlikely that the events recorded by Lee *et al.* consists solely of *neutral* particle colliding with clusters of charged particles, a further series of simulations were run to model collisions with single *charged* particles at a relative velocity of 0.06 m s^{-1}. However, preliminary calculations showed that it was necessary to reduce the magnitude of the charge on the single particle (initially $+5.2.10^6$ e) by a factor of three or four in order to improve the chances of observing capture. From figure 1b of Ref. 34, it can be seen that there is a high probability that experiments could involve particles that carry a lower charge than has been considered above. Figure 9a shows the consequences of a collision between a single particles with a charge of $1.7.10^6$ e and a cubic cluster with four negatively ($-5.2.10^6$ e) and four positively ($+5.2.10^6$ e) charged particles. As the particle becomes incorporated into the cluster, the collision cause two negatively charged particles to be expelled, but eventually one particle is attracted back into the structure. The final geometry seen after 800 ms has a ring-like structure of alternating positively and negatively charged particles and carries a net negative charge. The final panel in figure 9a shows this latter structure to be significantly less stable than the starting configuration. Figure 9b show the outcome of a collision where the charge on the colliding particle has been further reduced to $1.3.10^6$ e. Once again, two negatively charged particles are expelled, but this time the Coulomb and polarisation forces are strong enough to restore them to the aggregate and successfully complete the capture process. However, the final structure is again less stable than that of the starting geometry.

Most of the clusters of charged particles examined by Lee *et al.* [34] did not have the very stable, regular cubic structure selected for the simulations discussed above. In order to

examine how effective a less stable structure might be at capturing a particle, a series of simulations were run using geometries that were themselves generated through initial particle-cluster collisions. Taking, for example, the final structure shown in figure 7, it can be seen that this has more or less achieved a minimum energy after 800 ms, but is still about 6pJ less stable than the starting geometry. Despite numerous calculations, none of the metastable structures examined showed any evidence of being able to capture additional single particles.

Since the experiments of Lee *et al.* clearly show the capture of particles by irregular structures, one further modification was made to the calculations in order to try and initiate such a process. Figure 10 shows the sequence of events that follow a doubly collision. As before the cube consists of eight particles carrying charges of $\pm$ $5.2.10^6$ e, and in the first instance this is in collision with a particle carrying a charge of $-5.2.10^6$ e at a relative velocity of 0.045 m s^{-1}. This leads to a disordered structure which is then the subject of a further collision at 0.045 m s^{-1} with a particle carrying a change of $+5.2.10^6$ e; however, coincident with this collision the value taken for CR has been reduced from 0.94 to 0.74. It is clear from a plot of the interaction energy that the structure generated by the first collision relaxes close to an energy minimum for that particular metastable geometry, and that any residual internal energy is unlikely to make a significant contribution to further dissociation following a second collision. However, only through a reduction in the value of CR does it become possible for the simulations to reproduce particle capture by these more disordered structures.

In a final calculation, the calculations explore an observation by Lee *et al.* [34] that stable triangular geometries evolve when two particles with the same magnitude of charge but with opposite polarities interact with a particle carrying a lesser charge. In an example taken from [34] (figures 4e and 4f), figure 11 shows how two particles of radii 150 μm and carrying charges of $+ 1.8.10^6$ e and $+0.2.10^6$ e, respectively, interact with a particle of radius 100 μm and with a charge of $-2.3.10^6$ e. N = 4 and k = 15. A plot of their interaction energy shows that,

in the absence of polarisation, this becomes increasingly less attractive as θ increases and the two positively charged particles move closer together. In contrast, the inclusion of polarisation terms creates a situation where there is an initial slight long-range repulsion between the positively charge particles, but as θ increases beyond 80° the polarisation of bound charge becomes significant and the three particles adopt a stable triangular configuration; one which matches exactly the experimental result [34].

From this series of simulations on collisions between single particles and small clusters, it is very clear that particle polarisability (dielectric constant) plays a major role in the outcome of individual trajectories. Where polarisability is absent, particles do not aggregate during low velocity collisions, and collisions can become very destructive as the relative velocity is increased. In contrast, it is shown that polarisability contributes towards clusters retaining particles following a collision. It is also evident that polarisability has a significant influence on the geometries adopted by captured particles, and the non-additivity of such interactions has been quantified [17]. Whilst there is, as before, qualitative agreement with experimental observations, it is clear that some aspects of the interpretation need further clarification, and the value assigned to the coefficient of restitution is an example.

4. Conclusion

A theory that takes into account the many-body interactions present in close-packed collections of charged particles has been used to model the dynamics of elementary electrostatic self-assembly processes. Simulations have successfully reproduced patterns of behaviour seen in two quite distinct experimental studies [29-34], both of which were undertaken in the "gas phase" but involved particles of very different size, composition, charge, and dielectric constant. As might be expected, the simulation of experiments which comprised of particles

with a high dielectric constant were found to be more sensitive to the inclusion of terms involving the polarisation of bound charge.

Although these simulations have addressed very specific topics, the work has broader implications with regard to other situations where dielectric particles have been observed to coalesce or aggregate under similar "gas phase" conditions. Laboratory experiments on the aggregation of tribocharged hydrocarbon particles have identified a mechanism by which grain dunes on Titan could resist interference from the prevailing wind [47], and studies undertaken on the Space Shuttle on quartz and volcanic ash particles have also shown how tribocharging can promote aggregation [48]. Indeed the latter experiments provided evidence for the formation of filaments with estimated mean lengths of five particles, which is not unlike the behaviour seen above in figures 5, 8b and 10.

Authors' contributions. BS, YM, and EBL developed the theory and wrote the computer code. EBL undertook the calculations. AJS, EB, and EBL interpreted the data. The preparation of figures and writing the paper was mostly undertaken by AJS and EBL with critical input from the remaining authors. All authors have reviewed the final manuscript.

Acknowledgements. EBL is supported by a PhD scholarship from the Brazilian Government's Science Without Borders programme (CAPES: 0702/13-7). Part of this work (associated with YM and BS) has benefited from French state funding managed by CALSIMLAB and the ANR within the Investissements d'Avenir programme under reference ANR-11-IDEX-0004-02. EB acknowledges the financial support of an ERC Consolidator grant. AJS would like to thank the Leverhulme Trust for the award of an Emeritus Fellowship.

Table 1.

Whitesides and co-workers				
Particle type	Dielectric constant (*k*)	Radius (mm)	Density (kg m^{-3})	Charge (nC)
PMMA	3.2	1.59	1190	+0.31
Teflon	2.1	1.59	2280	-0.31; -0.93
Lee *et al*.				
ZrO_2/SiO_2 composite	15	0.15	3800	#

See text for details of individual examples.

References.

1. Shevchenko EV, Talapin DV, Kotov NA, O'Brien S. Murray CB. 2006 Structural diversity in binary nanoparticle superlattices. *Nature* **439**, 55-59. (doi: 10.1038/nature04414)

2. Sun S, Murray CB, Weller D, Folks L, Moser A. 2000 Monodispersed FePt nanoparticles and ferromagnetic FePt nanocrystal superlattices. *Science* **287**, 1989-1992. (doi: 10.1126/science.287.5460.1989)

3. Shevchenko EV, Talapin DV, Murray CB, O'Brien S. 2006 Structural Characterization of self-assembled multifunctional binary nanoparticle superlattices. *J. Am. Chem. Soc.* **128**, 3620-3637. (doi: 10.1021/ja0564261)

4. Liu S, Kurth DG, Möhwald H, Volkmer D. 2002 A thin-film electrochromic device based on a polyoxometalate cluster. *Adv. Mat.* **14**, 225-228. (doi: 10.1002/1521-4095(20020205)14:3<225::AID-ADMA225>3.0.CO;2-F)

5. Abécassis B. 2016 Three-dimensional self assembly of semiconducting colloidal nanocrystals: From fundamental forces to collective optical properties. *ChemPhysChem* **17**, 618-631. (doi: 10.1002/cphc.201500856)

6. Schoeler B, Kumaraswamy G, Caruso F. 2002 Investigation of the influence of polyelectrolyte charge density on the growth of multilayer thin films prepared by the layer-by-layer technique. *Macromolecules* **35**, 889-897. (doi: 10.1021/ma011349p)

7. Xia YS, Nguyen TD, Yang M, Lee B, Santo A, Podsiadlo P, Tang ZY, Glotzer SC, Kotov NA. 2011 Self-assembly of self-limiting monodisperse supraparticles from polydisperse nanoparticles. *Nature Nanotech.* **6**, 580-587. (doi: 10.1038/NNANO.2011.121)

8. Lee H, You S, Pikhitsa PV, Kim J, Kwon S, Woo CG, Choi M. 2011 Three-dimensional assembly of nanoparticles from charged aerosols. *Nano Lett.* **2011**, 119-124. (doi: 10.1021/nl103787k)

9. Iwafuji Y, McNamee, CE. 2012 Use of attractive forces to create a self-assembled film of charged nanoparticles with a controlled packing. *Colloid and Surfaces A: Physicochem. Eng. Aspects* **398**, 24-31. (doi: 10.1016/j.colsurfa.2012.02.004)

10. Xu ZL. 2013 Electrostatic interaction in the presence of dielectric interfaces and polarization-induced like-charge attraction. *Phys. Rev. E* **87**, 013307. (doi: 10.1103/PhysRevE.87.013307)

11. Barros K, Sinkovits D, Luijten E. 2014 Efficient and accurate simulation of dynamic dielectric objects. *J. Chem. Phys.* **140**, 064903. (doi: 10.1063/1.4863451)

12. Gan, ZC, Wu HX, Barros K, Xu ZL, Luijten E. 2015 Comparison of effective techniques for the simulation of dielectric objects in electrolytes. *J. Comp. Phys.* **291**, 317-333. (doi: 10.1016/j.jcp.2015.03.019)

13. Freed KF. 2014 Perturbative many-body expansion for electrostatic energy and field for systems of polarizable charged spherical ions in a dielectric medium. *J. Chem. Phys.* **141**, 034115. (doi: 10.1063/1.4890077)

14. Qin, J, de Pablo JJ, Freed KF. 2016 Image method for induced surface charge from many-body system of dielectric spheres. *J. Chem. Phys.* **145**, 124903. (doi: 10.1063/1.4962832)

15. Qin J, Li JY, Lee V, Jaeger H, de Pablo JJ, Freed KF. 2016 A theory of interactions between polarizable dielectric spheres. *J. Coll. Interface Sci.* **469**, 237-241. (doi: 10.1016/j.jcis.2016.02.033)

16. Gan ZC, Jiang SD, Luijten E, Xu ZL. 2016 A hybrid method for systems of closely spaced dielectric spheres and ions. *SIAM J. Sci. Comput.* **38**, B375-B395. (doi: 10.1137/15M105046X)

17. Lindgren EB, Stace AJ, Polack E, Maday Y, Stamm B, Besley E. 2017 An integral approach to calculate electrostatic interactions in many-body dielectric systems. *J. Comp. Phys. Submitted for publication.*

18. Zhang D, González-Mozuelos P, de la Cruz MO. 2010 Cluster formation by charged nanoparticles on a surface in aqueous solution. *J. Phys. Chem. C* **114**, 3754-3762. (doi: 10.1021/jp9085238)

19. Li Y, Zhang XR, Cao DP. 2013 Self-assembly of patterned nanoparticles on cellular membranes: Effect of charge distribution. *J. Phys. Chem. B* **117**, 6733-6740. (doi: 10.1021/jp312124x)

20. Šindelka K, Limpouchová Z, Lìsal M, Procházka K. 2014 Dissipative particle dynamics study of electrostatic self-assembly in aqueous mixtures of copolymers containg one neutral water-soluble block and one either positively or negatively charged polyelectrolyte block. *Macromolecules* **47**, 6121-6134. (doi: 10.1021/ma501018x)

21. Suttipong M, Grady BP, Striolo A. 2014 Self-assembled surfactants on patterned surfaces: Confinement and cooperative effects on aggregate morphology. *Phys. Chem. Chem. Phys.* **16**, 16388-16398. (doi: 10.1039/c4cp00882k)

22. Nie SY, Zhang XF, Gref R, Couvreur P, Qian Y, Zhang LJ. 2015 Multilayer nanoparticles self-assembled from opposite charged blends: Insights from mesoscopic simulation. *J. Phys. Chem C* **119**, 20649-20661. (doi: 10.1021/acs.jpcc.5b03833)

23. Mao RF. Lee M-T, Vishnyakov A, Neimark AV. 2015 Modeling aggregation of ionic surfactants using a smeared charge approximation in dissipative particle dynamics simulations. *J. Phys. Chem. B* **119**, 11673-11683. (doi: 10.1021/acs.jpcb.5b05630)

24. Procházka K, Šindelka K, Wang X, Limpouchová Z, Lìsal M. 2016 Self-assembly and co-assembly of block polyelectrolytes in aqueous solutions. Dissipative particle dynamics with explicit electrostatics. *Mol. Phys.* **114**, 307-3092. (doi: 10.1080/00268976.2016.1225130)

25. Dahirel V, Jardat M, Dufréche J-F, Turq P. 2007 New coarse-graining procedure for the dynamics of charged spherical nanoparticles in solution. *J. Chem. Phys.* **126**, 114108. (doi: 10.1063/1.2710254)

26. Dahirel V, Jardat M, Dufréche J-F, Turq P. 2008 Ion-mediated interactions between charged and neutral nanoparticles. *Phys. Chem. Chem. Phys.* **10**, 5147-5155. (doi: 10.1039/b806315j)

27. Groot RD. 2003 Electrostatic interactions in dissipative particle dynamics – simulation of electrolytes and anionic surfactants. *J. Chem. Phys.* **118**, 11265. (doi: 10.10663/1.1574800)

28. Gavrilov AA, Chertovich AV, Kramarenko EY. 2016 Dissipative particle dynamics for systems with high density of charges: Implementation of electrostatic interactions. *J. Chem. Phys.* **145**, 174101. (doi: 10.1063/1.4966149)

29. Gryzbowski BA, Winkleman A, Wiles JA, Brumer Y, Whitesides GM. 2003 Electrostatic self-assembly of macroscopic crystals using contact electrification. *Nature Materials* **2**, 241-245. (doi: 10.1038/nmat860)

30. McCarty LS, Winkleman A, Whitesides GM. 2007 Electrostatic self-assembly of polystyrene microspheres using chemically directed contact electrification. *Angew. Chem. Int. Ed.* **46**, 206-209. (doi: 10.1002/anie.200602914)

31. McCarty LS, Whitesides GM. 2008 Electrostatic charging due to separation of ions at interfaces: Contact electrification of ionic electrets. *Angew. Chem. Int. Ed.* **47**, 2188-2207. (doi: 10.1002/anie.200701812)

32. Cademartiri R, Stan CA, Tran VM, Wu E, Friar L, Vulis D, Clark LW, Tricard S, Whitesides GM. 2012 A simple two-dimensional model system to study electrostatic-self-assembly. *Soft Matter* **8**, 9771-9791. (doi: 10.1039/c2sm26192h)

33. Soh S, Liu H, Cademartiri R, Yoon HJ, Whitesides GM. 2014 Charging of multiple interacting particles by contact electrification. *J. Am. Chem. Soc.* **136**, 13348-13354. (doi: 10.1021/ja506830p)

34. Lee V, Waitukaitis SR, Miskin MZ, Jaeger HM. 2015 Direct observation of particles interactions and clustering in charged granular streams. *Nature Physics* **11**, 733-738. (doi: 10.1038/NPHYS3396)

35. Lindgren EB, Stamm B, Chan H-K, Maday Y, Stace AJ, Besley E. 2017 The effect of like-charge attraction on aerosol growth in the atmosphere of Titan. *Icarus* **291**, 245-253. (doi: 10.1016/j.icarus.2016.12.013)

36. Griffiths DJ. 2013 *Introduction to electrodynamics*. New York: Pearson, 4th edition. (ISBN: 9780138053260)

37. Jackson JD. 1999 *Classical electrodynamics* New York: Wiley, 3rd edition. (ISBN: 9780471309321)

38. Mazur E. 2014 *The principles and practice of physics.* New York: Pearson, 1st edition. (ISBN: 9780321961594)

39. Press WH, Teukolsky SA, Vetterling WT, Flannery BP. 1992 *Numerical recipes in Fortran 77: The art of scientific computing.* Cambridge: Cambridge University Press, 2nd edition. (ISBN: 9780521430647)

40. Foerster SF, Louge MY, Chang AH, Allia K. 1994 Measurements of the collision properties of small spheres. *Phys. Fluids* **6**, 1108-1115. (10.1063/1.868282)

41. Bolintineanu DS, Grest GS, Lechman JB, Pierce F, Plimpton SJ, Schunk PR. 2014 Particle dynamics modelling for colloid suspensions. *Comp. Part. Mech.* **1**, 321-356. (doi: 10.1007/s40571-014-0007-6)

42. Español P, Warren PB. 2017 Perspective: Dissipative particle dynamics. *J. Chem. Phys.* **146**, 150901. (doi: 10.1063/1.4979514)

43. Bichoutskaia E, Boatwright AL, Khachatourian A, Stace AJ. 2010 Electrostatic analysis of the interactions between charged particles of dielectric materials. *J. Chem. Phys.* **133**, 024105. (doi:10.1063/1.3457157)

44. Lindgren EB, Chan H-K, Stace AJ, Besley E. 2016 Progress in the theory of electrostatic interactions between charged particles. *Phys. Chem. Chem. Phys.* **18**, 5883-5895. (doi: 10.1039/c5cp07709e)

45. Stace AJ, Boatwright AL, Khachatourian A, Bichoutskaia E. 2011 Why like-charged particles of dielectric materials can be attracted to one another. *J. Coll. Interface Sci.* **354**, 417-420. (doi: 10.1016/j.jcis.2010.11.030)

46. Murrell JN, Bosanac SD 1989 *Introduction to the theory of atomic and molecular collisions*. Chichester: J. Wiley & Sons. (ISBN 0471923656)

47. Méndez Harper JS, McDonald GD, Dufek J, Malaska MJ, Bur DM, Hayes AG, McAdams J, Wray JJ. 2017 Electrification of sand on Titan and its influence on sediment transport. *Nature Geoscience* **10**, 260-265. (doi: 10.1038/NGEO2921)

48. Marshall JR, Sauke TB, Cuzzi JN. 2005 Microgravity studies of aggregation in particulate clouds. *Geophys. Res. Letts.* **32**, L11202. (doi: 10.1029/2005GL022567)

Figure captions.

Figure 1. Schematic depicting the geometric configuration of charge particles and the various labels assigned to the system. Definitions of the terms are given in the text.

Figure 2. Time-dependent behaviour of two oppositely charged particles trapped in an attractive well defined by Coulomb and charge-induced interactions, where the latter depend on the value of the dielectric constant, *k*. Figure 2a, CR=1 with no energy dissipation; Figure 2b CR=0.94.

Figure 3. Timed images taken from a small-scale simulation of an experiment by Whitesides and co-workers [29-33]. The green/yellow spheres represent PMMA particles with a diameter of 1.59 mm and a charge of +0.31 nC and the blue spheres represent Teflon particles with a diameter of 1.59 mm and a charge of -0.31 nC. Changes in colour denote difference in surface charge density, with yellow on the more polarisable PMMA particles (k=3.2) representing regions of highest density. Changes in colour on the less polarisable Teflon particles (k=2.1) are not as evident. The numbers at the top of each panel are the maximum recorded surface charge densities in units of nC mm^{-2}. The final panel shows the time evolution of the interaction energy of the system in μJ and the Root Mean Square velocity of the particles in m s^{-1}.

Figure 4. As for figure 3, but for 36 PMMA particles and 12 Teflon particles and where the latter carry a charge of -0.93 nC.

Figure 5. As for figure 3, but for 36 PMMA particles and 12 Teflon particles and where the latter carry a charge of -0.31 nC.

Figure 6. Timed images taken from the simulation of a collision at a relative velocity of 0.04 m s^{-1} between a single *neutral* particle and a cube composed of eight ZrO_2 / SiO_2 particles. The yellow particles carry a charge of $+5.2.10^6$ e and the blue particles a charge of $-5.2.10^6$ e. Changes in shading denote regions of differing surface charge density, with deep yellow and deep blue representing the highest densities and the numbers at the top of each panel are the maximum recorded surface charge densities in units of e μm^{-2}. The final panel shows the time evolution of the interaction energy of the system in pJ and the Root Mean Square velocity of the particles in ms^{-1}; the time at which the collision occurs is denoted by a yellow sphere. In Fig 6a, k=1 and in Fig 6b, k=15.

Figure 7. As for figure 6, but with a relative velocity of 0.06 m s^{-1}. In Fig 7a, k=1 and in Fig 7b, k=15.

Figure 8. As for figure 6, but with a relative velocity of 0.08 m s^{-1}. In Fig 8a, k=1 and in Fig 8b, k=15.

Figure 9. As figure 6, but where the colliding particle carries a positive charge of either $+1.7.10^6$ e (figure 9a) or $+1.3.10^6$ e (figure 9b) and k=15.

Figure 10. As for figure 6, but for the sequence of events following a double collision. The first particle carries a charge of $-5.2.10^6$ e and CR has a value of 0.94. For the second collision the particle carries a change of $+5.2.10^6$ e and the value of CR has been reduced to 0.74.

Figure 11. Plot of the calculation the calculated interaction energy between three charged particles as a function of the angle θ as defined in the figure. Two particles have radii of 150

μm and carry charges of + $1.8.10^6$ e and +$0.2.10^6$ e, respectively, and the third has a radius of 100 μm and a charge of -$2.3.10^6$ e. N = 4 and k = 15.

Figure 1

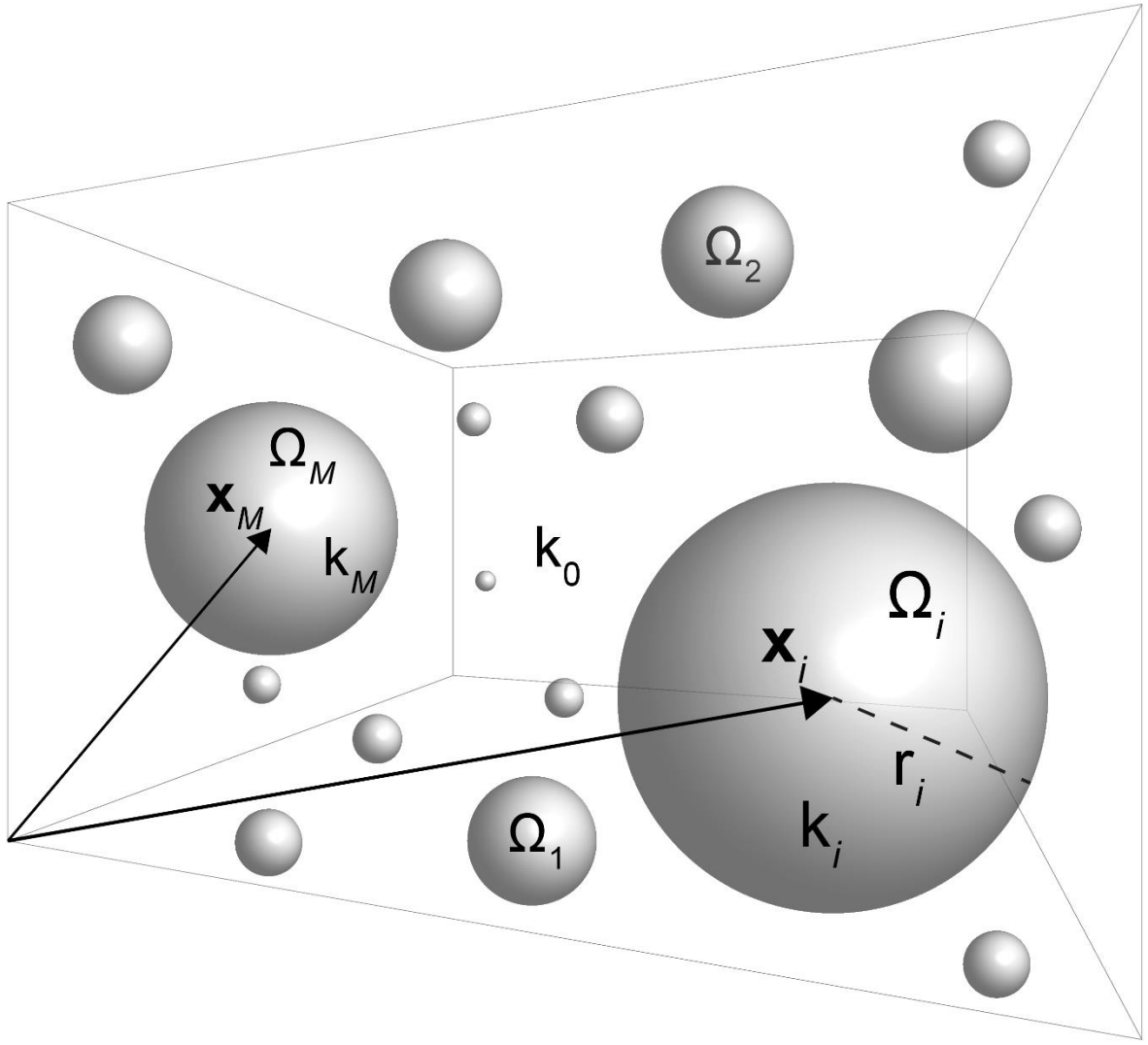

Figure 2a

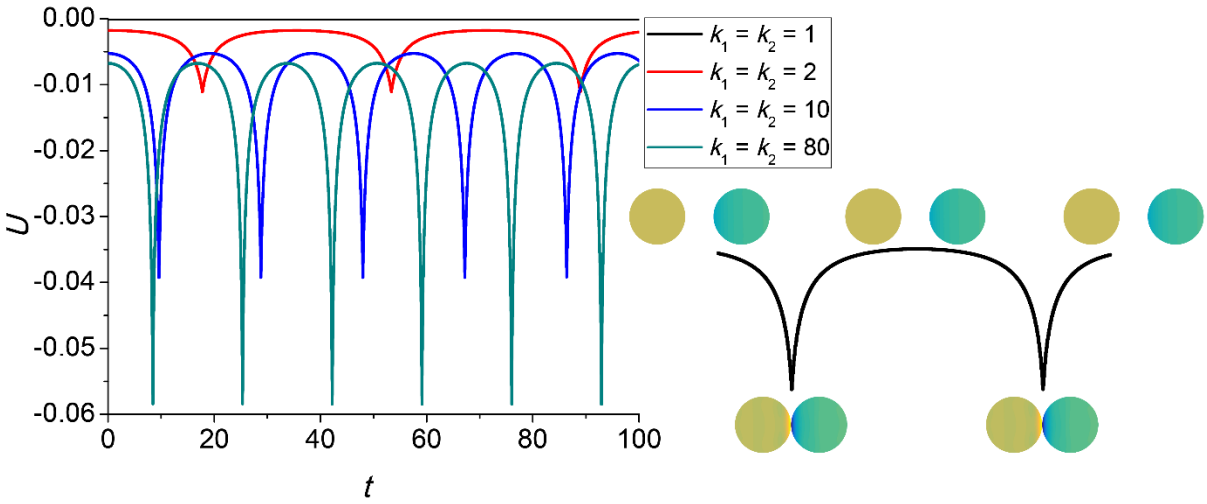

Figure 2b

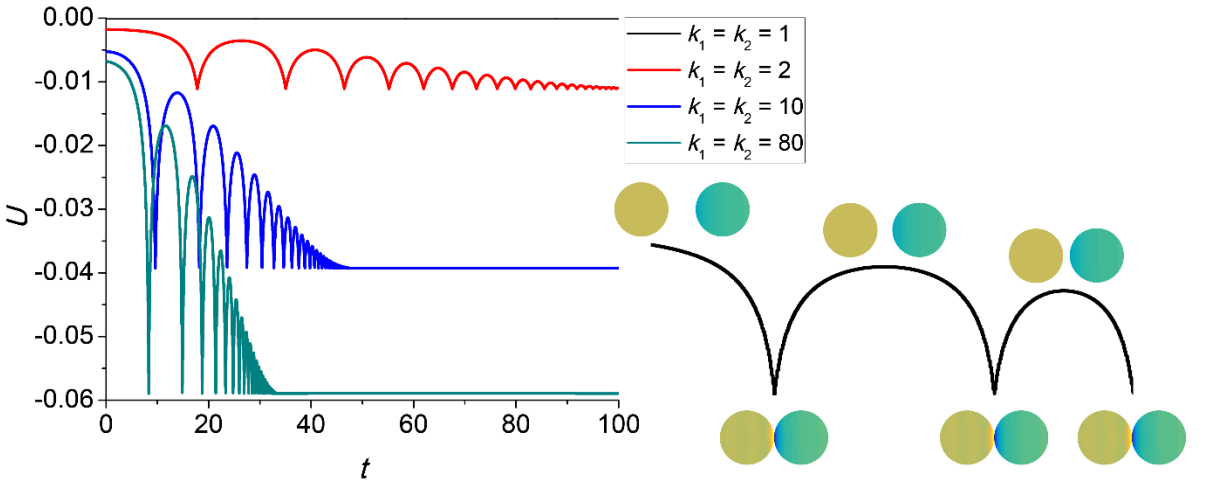

Figure 3

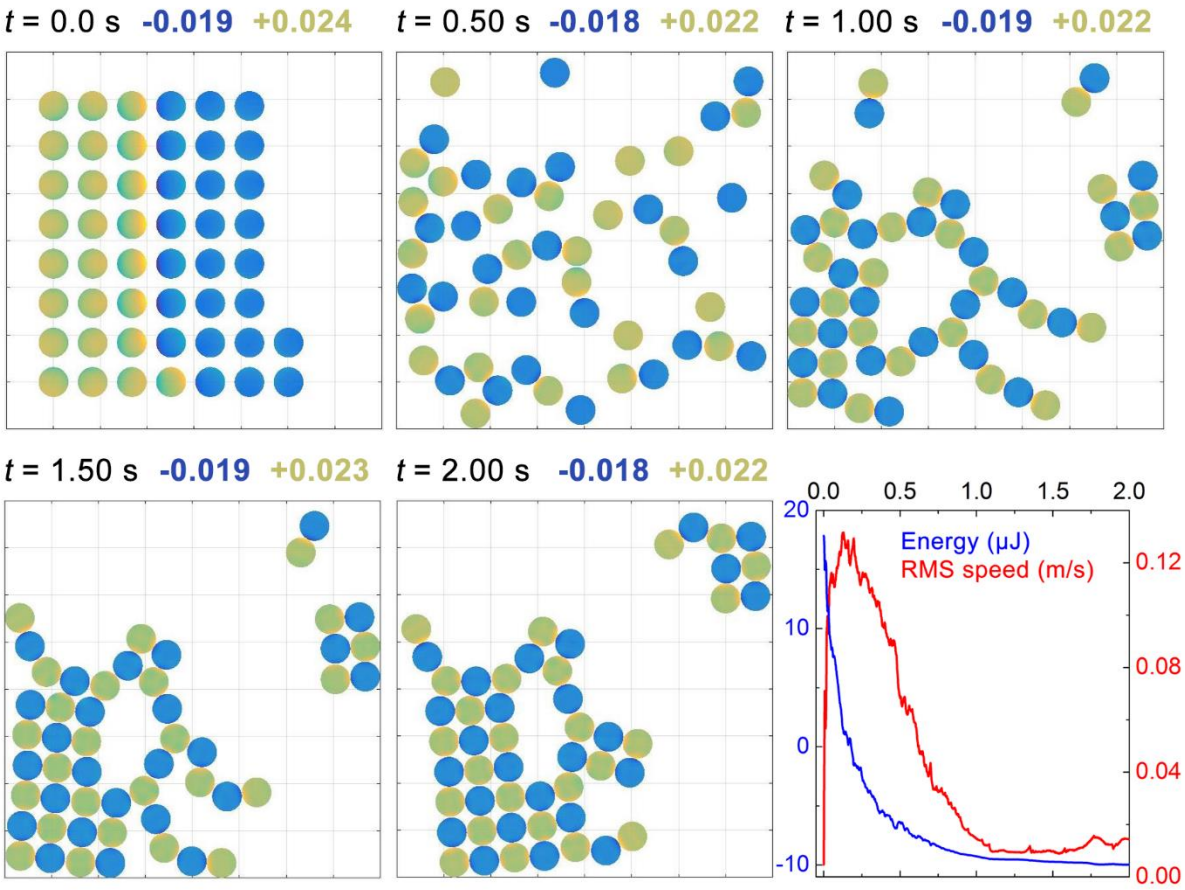
t = 0.0 s -0.019 +0.024
t = 0.50 s -0.018 +0.022
t = 1.00 s -0.019 +0.022
t = 1.50 s -0.019 +0.023
t = 2.00 s -0.018 +0.022
0.0 0.5 1.0 1.5 2.0
20
10
0
-10
Energy (μJ)
RMS speed (m/s)
0.12
0.08
0.04
0.00

Figure 4

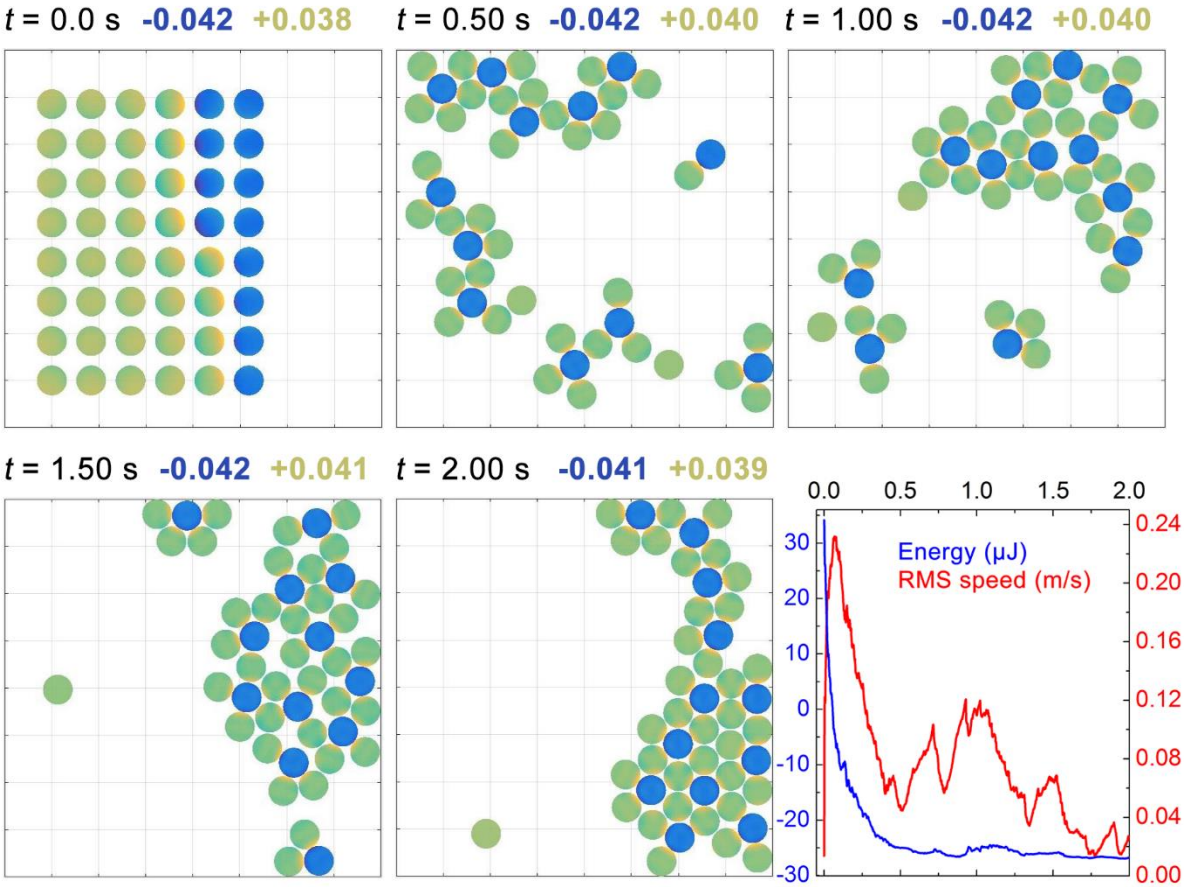
t = 0.0 s -0.042 +0.038
t = 0.50 s -0.042 +0.040
t = 1.00 s -0.042 +0.040
t = 1.50 s -0.042 +0.041
t = 2.00 s -0.041 +0.039
0.0 0.5 1.0 1.5 2.0
30 20 10 0 -10 -20 -30
0.24 0.20 0.16 0.12 0.08 0.04 0.00
Energy (μJ)
RMS speed (m/s)

Figure 5

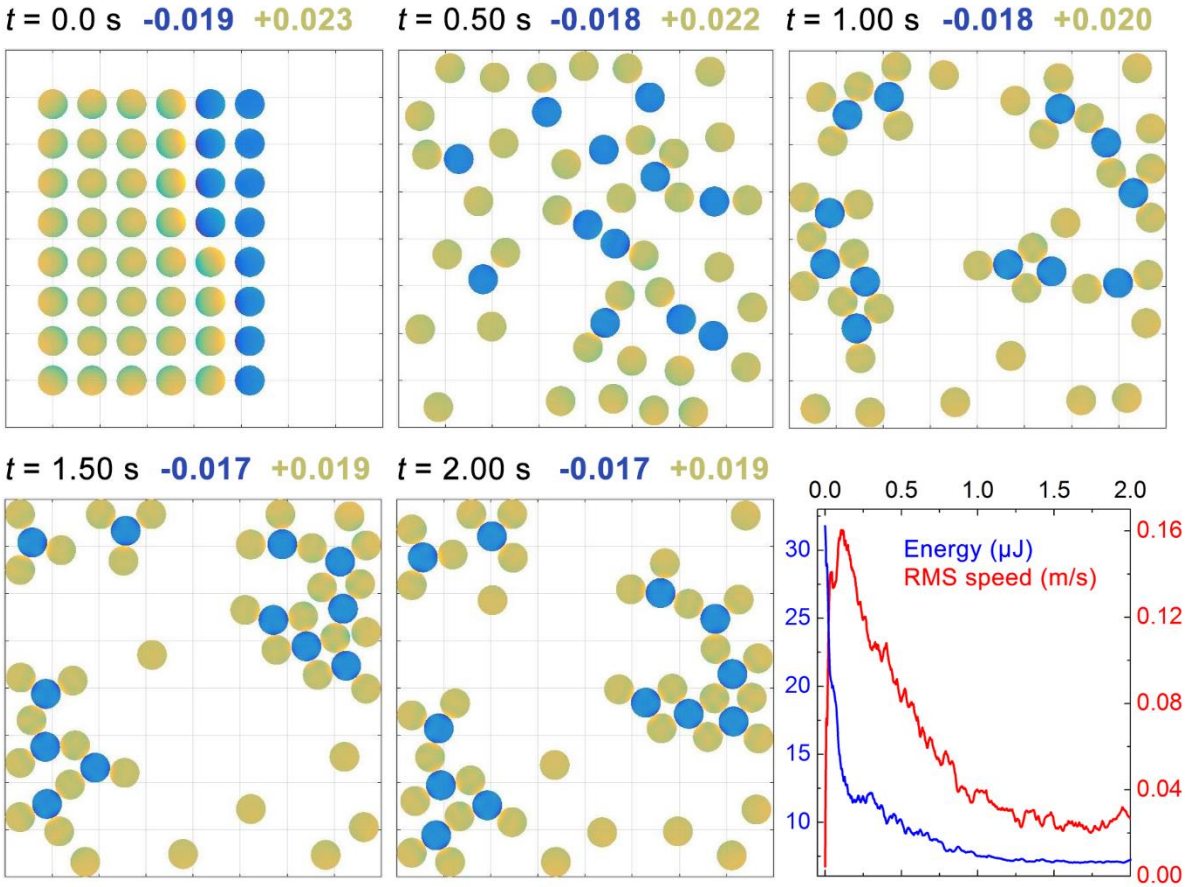
t = 0.0 s -0.019 +0.023
t = 0.50 s -0.018 +0.022
t = 1.00 s -0.018 +0.020
t = 1.50 s -0.017 +0.019
t = 2.00 s -0.017 +0.019
0.0 0.5 1.0 1.5 2.0
30 25 20 15 10
0.16 0.12 0.08 0.04 0.00
Energy (μJ)
RMS speed (m/s)

Figure 6a

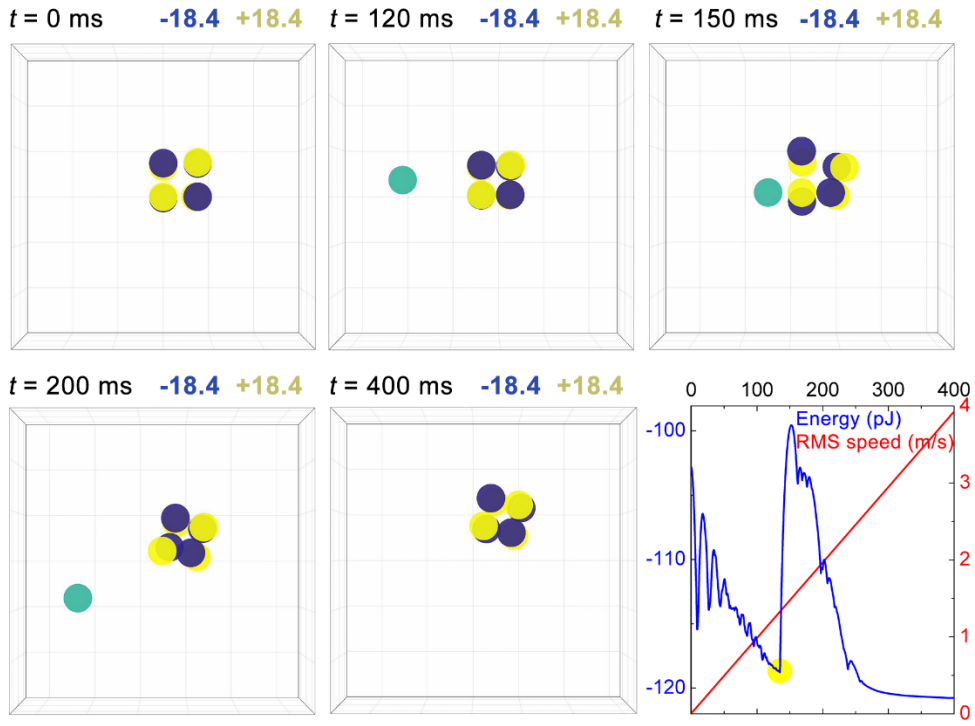

Figure 6b

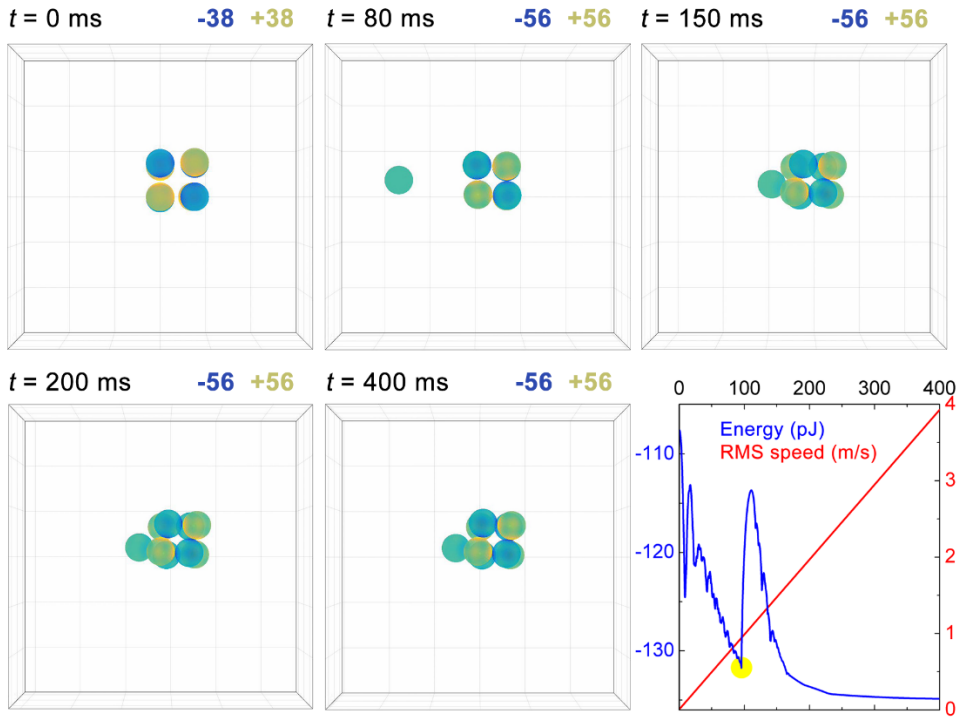

Figure 7a

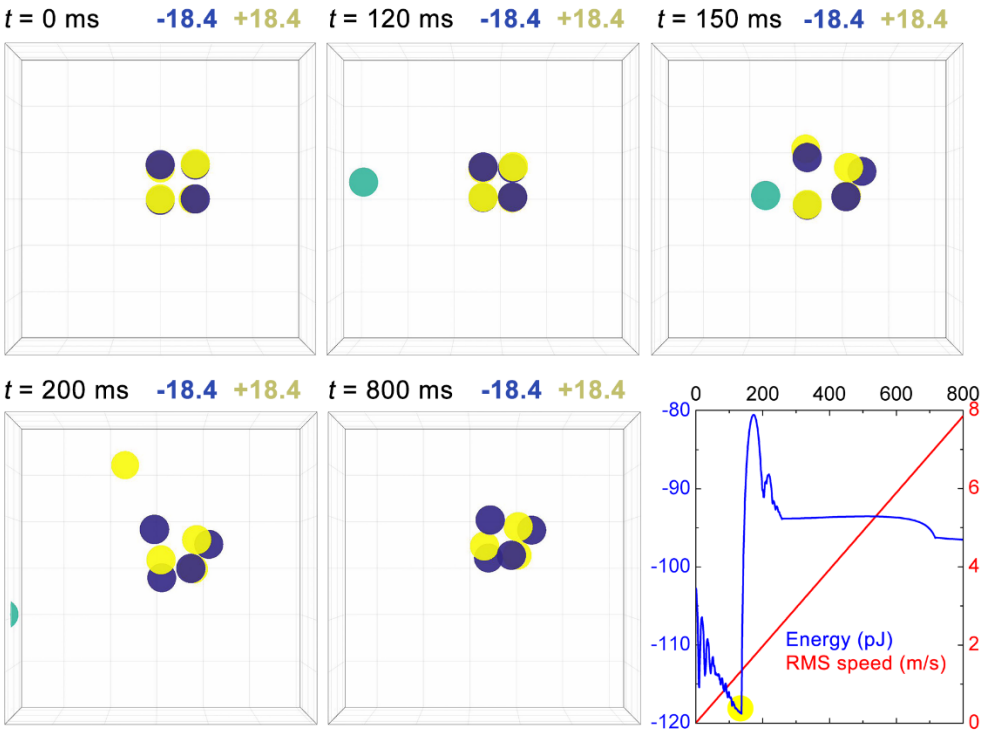

Figure 7b

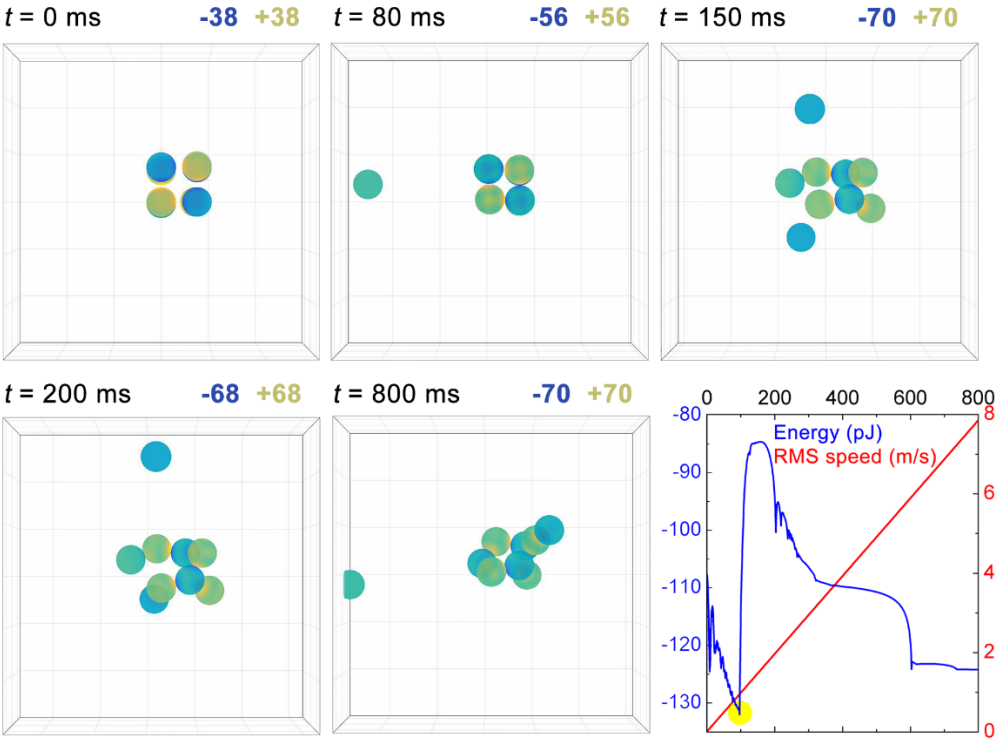

Figure 8a

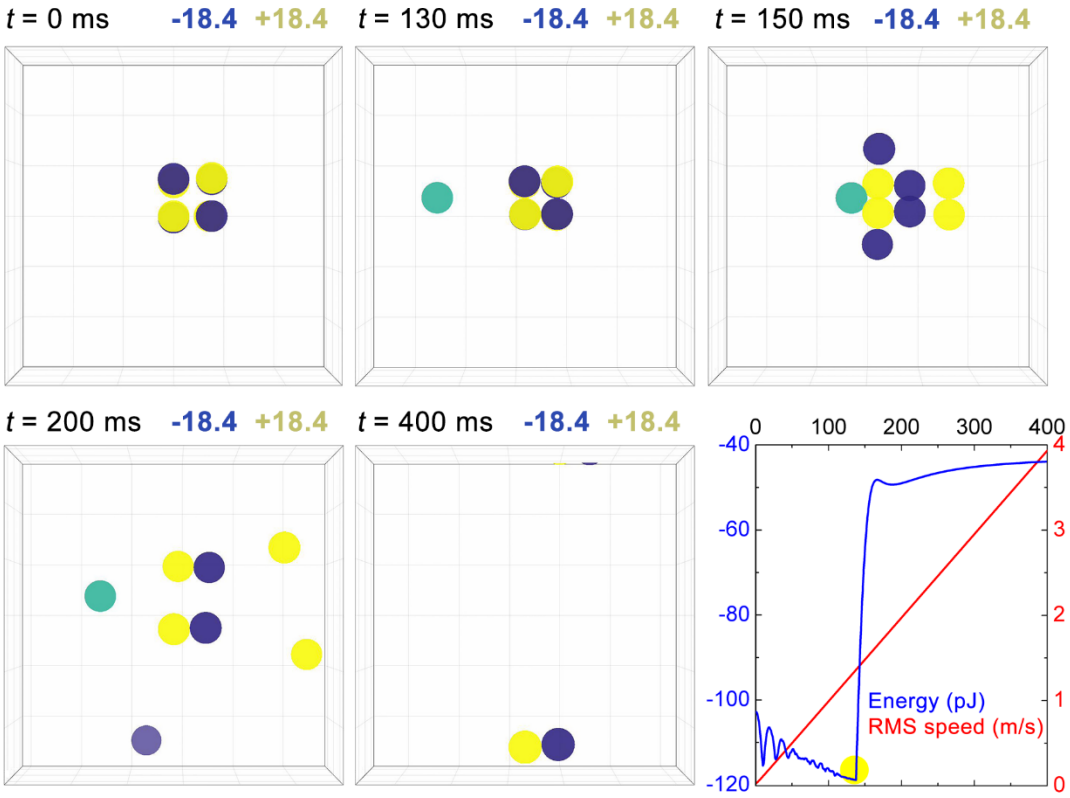

Figure 8b

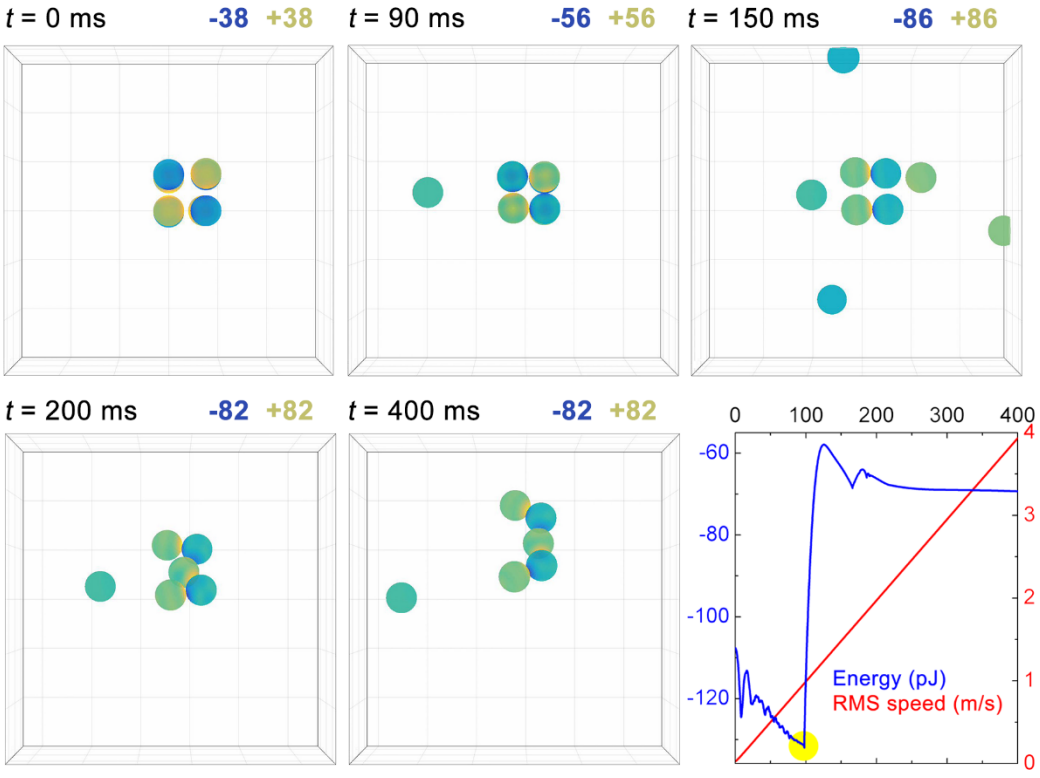

Figure 9a.

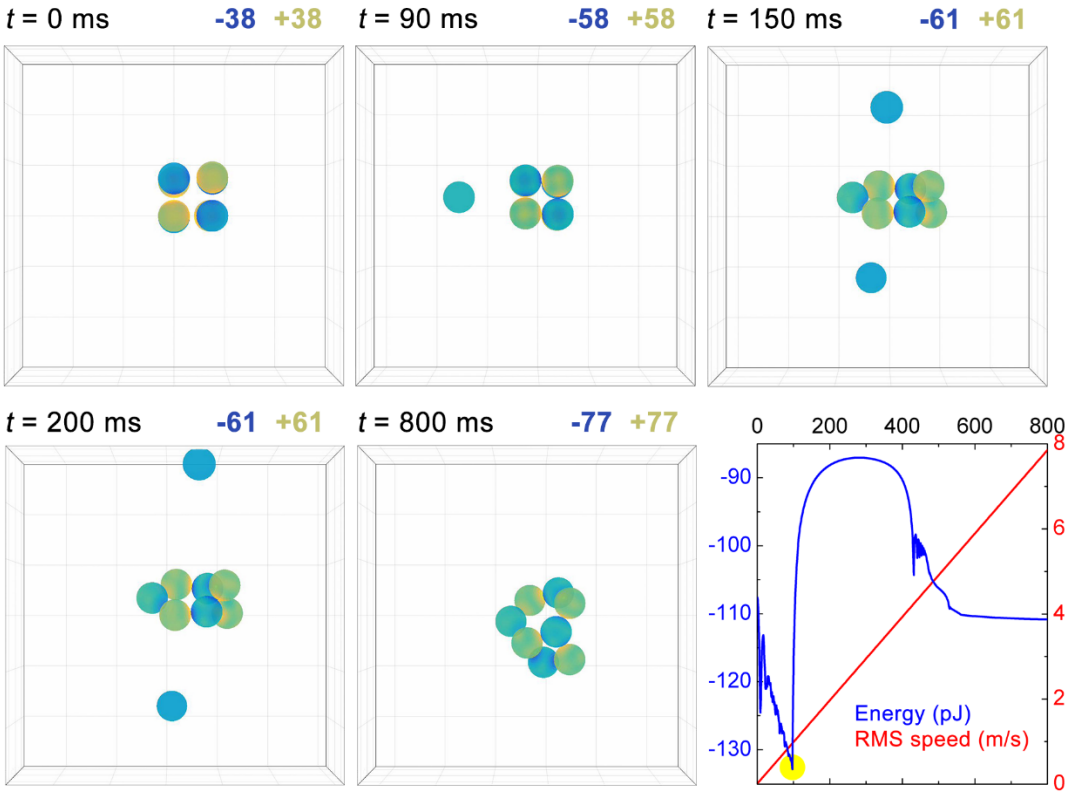

Figure 9b

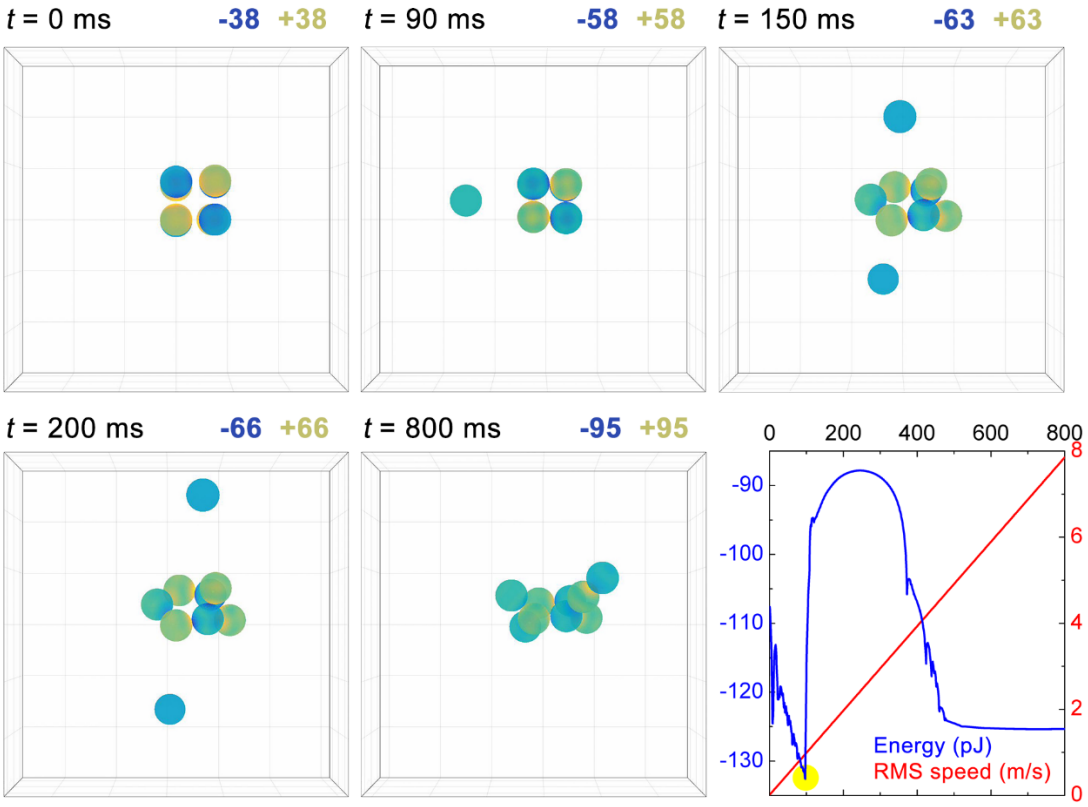

Figure 10.

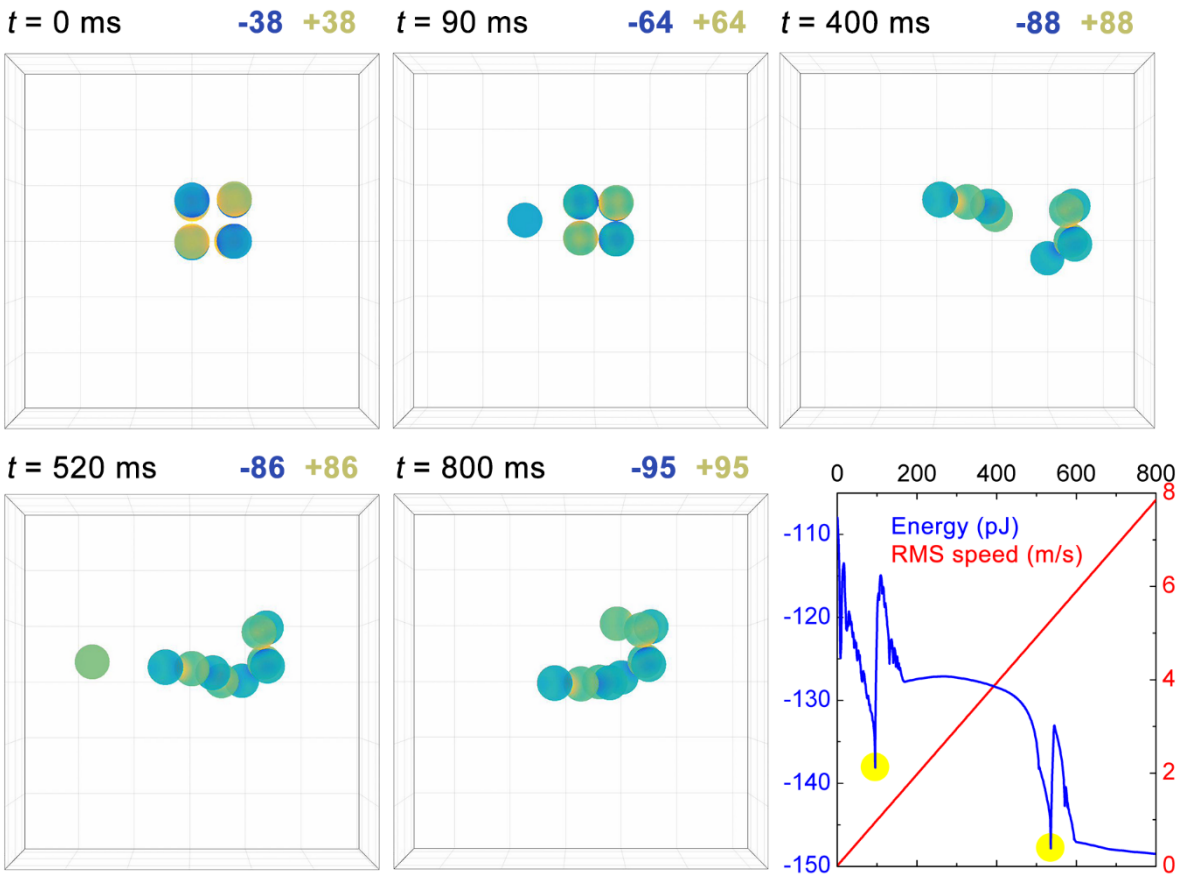
t = 0 ms
-38 +38
t = 90 ms
-64 +64
t = 400 ms
-88 +88
t = 520 ms
-86 +86
t = 800 ms
-95 +95
0
200
400
600
800
-110
-120
-130
-140
-150
8
6
4
2
0
Energy (pJ)
RMS speed (m/s)

Figure 11.

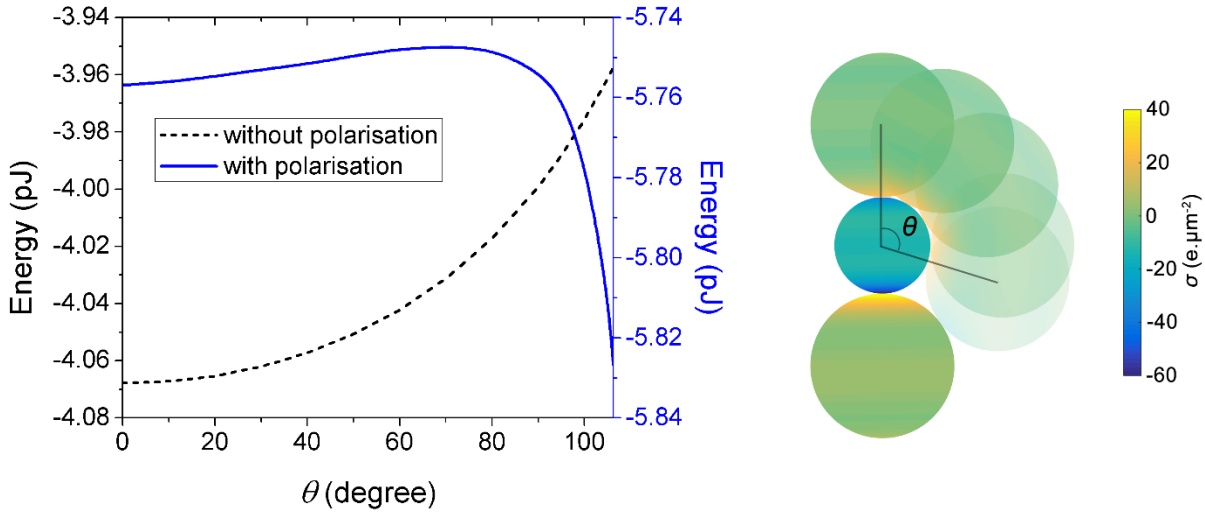
-3.94
-3.96
-3.98
-4.00
-4.02
-4.04
-4.06
-4.08
Energy (pJ)
-5.74
-5.76
-5.78
-5.80
-5.82
-5.84
Energy (pJ)
without polarisation
with polarisation
0
20
40
60
80
100
θ (degree)
θ
40
20
0
-20
-40
-60
σ (e.µm-2)